ACS OMEGA

http://pubs.acs.org/journal/acsodf

Article

Host–Guest Encapsulation of RIBO with TSC4X: Synthesis, Characterization, and Its Application by Physicochemical and Computational Investigations

Biswajit Ghosh, Niloy Roy, Saikat Mandal, Salim Ali, Pranish Bomzan, Debadrita Roy, Md Salman Haydar, Vikas Kumar Dakua, Anupam Upadhyay, Debabrata Biswas, Kausik Kumar Paul, and Mahendra Nath Roy*

Cite This: *ACS Omega* 2023, 8, 6778–6790

Read Online

ACCESS | Metrics & More | Article Recommendations | Supporting Information

ABSTRACT: In our present work, we synthesized a new encapsulated complex denoted as RIBO-TSC4X, which was derived from an important vitamin riboflavin (RIBO) and *p*-sulfonatothiacalix[4]arene(TSC4X). The synthesized complex RIBO-TSC4X was then characterized by utilizing several spectroscopic techniques such as ^{1}H-NMR, FT-IR, PXRD, SEM, and TGA. Job's plot has been employed to show the encapsulation of RIBO (guest) with TSC4X (host) having a 1:1 molar ratio. The molecular association constant of the complex entity (RIBO-TSC4X) was found to be 3116.29 ± 0.17 M^{-1}, suggesting the formation of a stable complex. The augment in aqueous solubility of the RIBO-TSC4X complex compared to pure RIBO was investigated by UV–vis spectroscopy, and it was viewed that the newly synthesized complex has almost 30 times enhanced solubility over pure RIBO. The enhancement of thermal stability upto 440 °C for the RIBO-TSC4X complex was examined by TG analysis. This research also forecasts RIBO's release behavior in the presence of CT-DNA, and at the same time, BSA binding study was also carried out. The synthesized RIBO-TSC4X complex exhibited comparatively better free radical scavenging activity, thereby minimizing oxidative injury of the cell as evident from a series of antioxidant and anti-lipid peroxidation assay. Furthermore, the RIBO-TSC4X complex showed peroxidase-like biomimetic activity, which is very useful for several enzyme catalyst reactions.

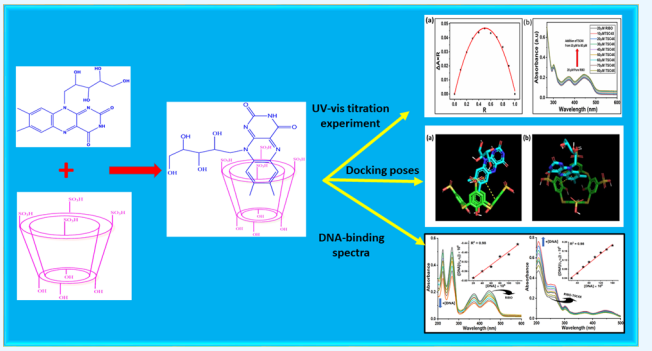

1. INTRODUCTION

Riboflavin (RIBO) which is 7,8-dimethyl-10-(1′-D-ribityl)-isoalloxazine belongs to the Flavin family,[1] commonly known as vitamin B2. RIBO is a very essential compound to initiate major cellular processes, especially because it is associated with various redox processes and biological electron transport. RIBO is extensively utilized in the field of medicine and food chemistry.[2] Basically, RIBO is a yellow-orange colored naturally occurring fluorescent pigment indispensable as a human nutrient.[3] The genesis of the yellow-orange color of RIBO is mainly due to the absorption of visible light (λ_{max} = 446 nm). It is predominantly found with a reasonably high concentration in food items such as meat, milk, fatty fish, some fruits and green vegetable, and in aerobic organisms.[4] RIBO subsists as an orange-yellow crystal that is stable toward heat, acid, or oxidation but it appears to be highly sensitive toward light, especially UV radiation of sunlight. Vitamin B2 can easily be absorbed in the body and mixed with blood, which supplies it to the tissues. However, if anyone consumes excess RIBO, it will be excreted from the body through urine in the form of other metabolites such as 7-hydroxymethyl riboflavin and lumiflavin, as they are water soluble substances.[5,6] RIBO is a nontoxic compound approved by the FDA, stored in the liver and kidney of humans in very small quantity. RIBO in an aqueous medium irradiated by sunlight will be converted into lumichrome under neutral condition and into lumiflavin in an alkaline solution.[7]

Two co-enzymes named flavin mononucleotide (FMN) and flavin adenine dinucleotide (FAD) have played important roles in energy production, and RIBO acts as the precursor to them. These co-enzymes transport hydrogen in order to help in making energy in the form of adenosine triphosphate (ATP) through the metabolism of carbohydrates and fats.[8] RIBO also

Received: November 18, 2022
Accepted: January 25, 2023
Published: February 7, 2023

shows its medicinal effect on those who are suffering from visionary-related issues (like eye burning and excess tearing), growth of the cells, skin, hair, and so forth. Riboflavin-5-phosphate can be assimilated readily instead of RIBO itself for people suffering from allergies and chemical sensitivities.[9] Alcohol-related problems, digestive difficulties, ulcers, and leg pain can also be eradicated with the help of RIBO. During cancer treatment, doctors often prescribe RIBO supplements to the patients.[10]

Recent observation reveals that humans do not consume sufficient RIBO despite having accessible RIBO-rich foods. The deficiency in RIBO intake may cause several health related problems such as sore tongue, cheilosis, and scaly rashes on the scrotum or vulva.[11,12] Its deficiency also causes night blindness, the lack of growth, mild anaemia, and fatigue. The scarcity of RIBO may also increase the risk of cancer and cardiovascular-like major diseases.[13] However, the majority of diseases caused due to the lack of RIBO intake in humans can be controlled by providing a normal diet with RIBO-associated supplements.[14,15] Generally, RIBO has poor aqueous solubility and high photosensitivity, as a result its medicinal and biological activity gets reduced.[16] Therefore, to enhance the aqueous solubility, photo stability, and biological activity of RIBO, it is encapsulated with *p*-sulfonatothiacalix[4]arene (TSC4X), a special type of host molecule that belongs to Calixarene class compounds.[17]

In supramolecular chemistry, if macrocycles are termed as pillars, then calixarenes are regarded as the third pillar after the well-investigated cyclodextrins and crown ethers. Calixarenes are viewed as one of the most significant classes of macrocyclic host compounds.[18] Calixarenes are the condensation product of phenol and aldehyde as many aromatic compounds can be derived from phenol, resorcinol, or pyrogallol.[19] Because of the flexible hydrophobic cavity, they have the ability to make rim modifications to incorporate specific guest molecules such as drugs, vitamins, and metal ions.[20] The *p*-sulfonatothiacalix[4]-arene (TSC4X), which is a derivative of calixarene, is composed of phenolic groups linked by the 'S' atom at the 2 and 6 positions. The sulfonated calixarenes from the calixarene family are less toxic, sufficiently soluble in water, and possess high stability.[21,22] It has been explored that the TSC4X compound finds application in the field of smart materials, drug delivery, chemical sensors, and molecular recognition owing to their nontoxic behavior and high selectivity and affinity for various kinds of guests in the aqueous medium.[23,24] The Π-stacking, electrostatic, and hydrophobic interacts provide stability when various guest molecules are complexed with TSC4X.[25] Hence, the fundamental investigations involving the interactions of sulfonated calixarenes with different types of guests are important for their advanced applications.

In the current work, we attempted to synthesize the encapsulated complex of guest molecule RIBO with the host molecule TSC4X, and the formation of the RIBO-TSC4X complex was characterized by using different spectroscopic methods such as ^{1}H-NMR, Fourier transform infrared (FT-IR) spectroscopy, thermogravimetric analysis (TGA), powder X-ray diffraction (PXRD), and scanning electron microscopy (SEM). UV−vis spectroscopy was employed to explain the 1:1 encapsulation ratio and obtain the association constant value along with thermodynamic parameters. A molecular modeling method was performed to highlight the possible interaction between RIBO and TSC4X. The molecular docking study displays the most stable orientation of binding interaction when RIBO is being inserted into the hydrophobic cavity of TSC4X. We have also explored the binding characteristics of the RIBO-TSC4X complex with CT-DNA and BSA, respectively, by employing spectroscopic techniques and also to determine the binding affinity of RIBO-TSC4X complex with CT-DNA and BSA. The bioactivity of the synthesized encapsulated complex was evaluated in terms of antioxidant and anti-lipid peroxidation activity as vitamin B2 is a potent but neglected antioxidant nutrient. The enzyme mimicking activity of synthesized RIBO-TSC4X complex has been investigated using peroxidase (POD) and compared with pure RIBO. This work aimed to improve the aqueous solubility, enhancement of bioactivity of the encapsulated complex compared to pure RIBO.

2. EXPERIMENTAL SECTION

2.1. Particulars of the Chemical Compounds. Both the chemicals RIBO with purity ≥99% and *p*-sulfonatothiacalix-[4]arene with purity ≥99% were procured from TCI Chemicals India Pvt. Ltd. All the other solvents required in the given investigation were HPLC grade. Exclusively pure doubly distilled water was used in every step of the experiment, and the particulars of the chemical purchased are summarized in Table S1.

2.2. Instruments. The mass of pure RIBO and TSC4X was weighed using a Shimadzu electronic balance with a ±0.01 mg uncertainty.

All the UV−visible spectra required for specific experiment were recorded using the Agilent 8453 spectrophotometer with ±2 nm uncertainty in wavelength. The temperature during the experiments was controlled by an automatic digital thermostat.

The ^{1}H-NMR spectra of the compounds viz pure RIBO, TSC4X, and RIBO-TSC4X encapsulated complex were recorded utilizing a Bruker Avance DRX 400 MHz NMR spectrometer. Approximately 4 mg of each sample was taken in a NMR tube and then dissolved in 1 mL of D_2O. The chemical shift values were measured in ppm unit.

The FT-IR spectra were recorded using KBr disc method on a Perkin-Elmer spectrometer with a 4 cm^{-1} in resolution. The spectral analysis was performed in the wavenumber range of 4000−400 cm^{-1}.

The extent of thermal stability of the samples was examined by TG analysis using a TA instrument Q-50 TGA in the temperature range of 30−600 °C with a heating rate of 10 °C per minute.

The surface morphology and particle size were investigated using a JSM-6360 scanning electron microscope.

Bruker D8 Advance instrument made in Germany having radiation source of a Cu Kα (45 KV & λ = 1.5406 Å) was used to acquire PXRD data and the samples were scanned in the range from 5 to 80°.

2.3. Synthesis of RIBO-TSC4X Complex. The synthesis of the solid RIBO-TSC4X complex from its pure components, namely, RIBO and TSC4X, with a 1:1 molar ratio was done by implementing a very common method usually known as the co-precipitation method.[26] In two separate beakers, RIBO and TSC4X were dissolved in 40 mL of H_2O. Then, the TSC4X solution was kept on a magnetic stirrer and RIBO solution was slowly added into it with moderate stirring for 1 h as long as they were fully mixed. The mixed solution was then heated at 55 °C temperature for about 70 h with constant stirring in order to have precipitated. After that, the resulting precipitate

https://doi.org/10.1021/acsomega.2c07396
ACS Omega 2023, 8, 6778−6790

was filtered and washed with EtOH to remove impurities. The purely obtained precipitate was then kept in an oven at 50 °C for 12 h. Finally, the solid RIBO-TSC4X complex was collected in the powder form and preserved in a desiccator for further investigation.[27]

2.4. Aqueous Solubility Study Procedure. The aqueous solubility of the RIBO-TSC4X complex was determined by preparing solutions at 25 °C having different concentrations (mg mL^{-1}) of (a) 0.033, (b) 0.066, (c) 0.099, (d) 0.132, (e) 0.165, (f) 0.198, and (g) 0.228. Thereafter, using an Agilent spectrophotometer, the UV−vis spectra of the above prepared solutions were recorded. Then, the absorbance against the concentration of RIBO-TSC4X was plotted, which gave a straight line as described in Figure 2a. Finally, using the formula of Lambert−Beer's law $A = \varepsilon Cl$ (where A = absorbance of the solutions, ε = absorption coefficient, C = concentration of the solutions, and l = optical path length), the absorption coefficient was evaluated as 0.3186 mL mg^{-1} cm^{-1} and the solubility of the complex was measured accordingly using the absorbance value for the UV−vis spectrum of the saturated solution of the complex.[28]

2.5. Molecular Docking Method. PyRx software was used to find the geometry of the inclusion complex and their binding energy.[29] It acts as a user interface where, several software such as AutoDockVina, AutoDock 4.2, Mayavi, Open Babel, and so forth are available. We used AutoDockVina wizard as docking software. All the structures of the aforementioned molecules were imported from PubChem (https://pubchem.ncbi.nlm.nih.gov). The input files host and guest in the.pdb format were changes to.pdbqt files using inbuilt Autodock of software. After preparing the files, they were subjected to docking using AutoDock Vina. Initially, a grid box was prepared around the host molecule having binding site center of 7.2986, 3.3164, and 16.9639 for the X, Y, and Z axes, respectively, as well as Grid box dimensions for X, Y, and Z conformations were reported to be 25, 25, and 25, respectively. The interaction between RIBO and the respective TSC4X was interpreted using the Lamarckian genetic algorithm (LGA). Once docking was performed, the binding affinity (kcal mol^{-1}) of various conformations of the host with the guest was calculated by the software.

2.6. DNA Binding Study. In this work, interaction of the drug molecule RIBO and the inclusion complex RIBO-TSC4X with CT-DNA was studied by UV−vis spectroscopic titration. The CT-DNA solution in tris−HCl buffer was prepared and the purity of DNA was verified by measuring the absorbance ratio at λ_{260} and λ_{280}. It was found that the absorbance ratio (A_{260}/A_{280}) is in between 2.00 and 1.80, suggesting that the DNA is protein free.[30] The concentration was measured by considering the molar extinction coefficient[31] (ε) as 6600 $M^{-1}cm^{-1}$ at 260 nm. The experiment was carried out by recording UV spectra of 20 μM RIBO or RIBO-TSC4X in the absence and presence of CT-DNA of various concentrations (20−120 μM).

2.7. BSA Binding Study. BSA (bovine serum albumin) is the most abundant plasma protein present in the circulatory system, which plays a vital role in the distribution and transportation of metal ions, hormones, nutrients, and drug molecules to specific organs or tissues in the body.[32] The binding aptitude measurement of complexes with BSA was performed with the help of UV−vis spectroscopic titration. A solution of BSA (10 μM) in Tris−HCl buffer was prepared and the UV−vis spectrum was taken. After that, BSA spectra were recorded in the presence of increasing concentrations (5−35 μM) of RIBO or RIBO-TSC4X.

2.8. Assessment of Antioxidant and Metal Chelation Activity. The antioxidant activity of RIBO and the encapsulated complex (RIBO-TSC4X) was evaluated using the following antioxidant test.

2.8.1. DPPH Radical Scavenging Assay. DPPH (2,2-diphenyl-1-picrylhydrazyl) radical scavenging activity is one of the extensively used in vitro antioxidant assay.[33] The estimation was done by mixing 200 μL of the studied sample to 1800 μL of 100 mM DPPH, followed by incubation at room temperature. After 30 min, the absorbance was recorded at 517 nm. The absorbance of control was also recorded by taking methanol instead of test samples. The following equation was used to calculate the inhibition percentage.

$$\text{Inhibition percentage} = [(A_c - A_s)/A_c] \times 100\%$$

where A_s is the absorbance of the test sample and A_c is the absorbance of the control.

2.8.2. $ABTS^+$ Radical Scavenging Assay. Protocol prescribed by Haydar et al. was used to determine the $ABTS^+$ [2′-azino-bis(3-ethylbenzothiazoline-6-sulfonic acid)] radical scavenging activity.[34] The studied sample (1 mL) was added to 2 mL of ABTS solution, and after 30 min of incubation, the absorbance of the formed solution was read at 734 nm. The inhibition percentage was determined using the same formula as stated above.

2.8.3. Superoxide Scavenging Assay. Superoxide radical scavenging activity was done following the methodology prescribed by Fu et al.[35] The reaction was carried out by mixing 1 mL of test sample with 1 mL of NADH solution (936 μmol/L), 1 mL of NBT solution (312 μmol/L), and 10 μL of PMS (120 μmol/L). The reactions were performed under fluorescent light and the decrease in absorbance was measured at 560 nm.

2.8.4. Ferric Reducing Antioxidant Power Assay. Ferric reducing antioxidant power (FRAP) activity of the tested samples was estimated following the protocol given by Moein et al.[36] For determination, 1 mL of studied sample was mixed with 2.5 mL of 200 mM potassium phosphate buffer (pH-6.6) and 2.5 mL of 1% potassium ferricyanide and the mixture was incubated at 50 °C for 20 min. Consequently, 2.5 mL of 600 mM trichloroacetic acid (TCA) was added to the mixture. After centrifugation at 3000 rpm for 10 min, the supernatant (2.5 mL) was taken and to that equal volume (0.5 mL) of distilled water and 6 mM ferric chloride was mixed. The absorbance was measured at 700 nm and FRAP activity of the studied samples was expressed in μg ascorbic acid equivalent (AAE) per millimolar compound.

2.8.5. Metal Chelating Activity. Spectrophotometric assay for ferrous ions (Fe^{2+}) chelation activity of the tested sample was carried out according to Gupta et al.[37] Test sample (400 μL) was mixed with methanol (1600 μL) and 2 mM of $FeCl_2$ (40 μL) and mixed well. Simultaneously, ferrozine (5 mM, 800 μL) was added to the existing mixture and after 10 min, the absorbance of the resultant solution was read at 562 nm.

2.9. Anti-Lipid Peroxidation Capability of RIBO-TSC4X. Anti-lipid peroxidation potentiality of RIBO and RIBO-TSC4X was estimated according to the standard TBARS method (Shabbir et al.[38]). Fresh liver samples of Wistar albino rats were collected from Cell and Molecular Biology Laboratory, University of North Bengal. The collected samples were homogenized using cold phosphate-buffered

https://doi.org/10.1021/acsomega.2c07396
ACS Omega 2023, 8, 6778−6790

saline (PBS, pH 7.4) in a pre-chilled mortar-pestle. The obtained homogenate was filtered through muslin cloth and the filtrate was then subjected to cold centrifugation for 8 min at 10,000 rpm, and after centrifugation, the supernatant was collected and stored in cold condition. For assessment, with 2.8 mL of liver extract, 100 μL of ferrous sulfate (15 mM) and 100 μL of test sample were added and the mixture solution was incubated for 30 min at 37 °C. After that, a small portion (1 mL) was taken from the mixture solution and to that 10% TCA (1.5 mL) solution was added. After incubated for 10 min, 0.67% TBA solution (1.5 mL) was added to the reaction mixture and test tubes were boiled for 30 min in a boiling water bath (at 80 °C). After heating, centrifugation was done at 10,000 rpm to obtain a clear solution. The absorbance of the upper layer was measured at 535 nm using Systronics spectrophotometer-169. A separate control set was prepared following the same methodology without adding the test sample. The anti-lipid peroxidation efficacy of the tested samples was calculated using the following formula and was expressed as IC_{50} value and inhibition percentage.

Inhibition percentage

= [(absorbance of control − absorbance of sample)

/absorbanceof control] × 100%

2.10.1. POD-like Activity. POD-like activity of the present nanocatalyst RIBO-TSC4X (IC) was evaluated using TMB as the chromogenic substrate with the addition of supplementary oxidant H_2O_2 in the Hac −NaAc buffer solution (pH −5) under ambient condition followed by our earlier reported method.[39] For the typical reaction, the RIBO-TSC4X complex (250 μM) was added in 380 μM TMB solution (Hac −NaAc buffer pH-5), followed by the addition of 20 mM H_2O_2. Then, the solution was incubated for 30 min and recorded the absorbance in UV−visible spectroscopy at 652 nm for monitoring the progress of the reaction. The optimum condition for best catalytic activity such pH (1−11) and time are also carried out.

2.10.2. Steady-State Kinetics. Steady-state kinetics of the RIBO-TSC4X complex (IC) for H_2O_2 was estimated under similar reaction conditions except that for the substrate H_2O_2 concentration were varying of 5, 10, 15, 20, 25, and 30 mM. All-important kinetics parameter like Km and Vmax are calculated using the linear plot derived from Michaelis Menten eq 1.[40]

$$V = V_{max}[S]/[S] + K_m \quad (1)$$

Here, V represents the average rate of conversion of a substrate, V_{max} is the maximum rate of conversion of a substrate, [S] stands for the substrate concentration, and K_m is the Michaelis constant. K_m is equal to the concentration of the substrate at which the rate of conversion becomes half of V_{max}. The Michaelis constant K_m represent the affinity (binding capacity) of an enzyme toward the substrate, and the low K_m value indicated the high affinity of an enzyme for the substrate.[41]

3. RESULTS AND DISCUSSION

3.1. Job's Plot to Determine the Stoichiometry of the RIBO-TSC4X Complex. The stoichiometric ratio of RIBO-TSC4X complexation between RIBO and TSC4X in an aqueous solution can be precisely determined by Job's method using UV−vis spectroscopy.[42] Job's method which is also commonly known as the continuous variation method was employed to evaluate the stoichiometry of an important vitamin RIBO and TSC4X. In this method, the pure RIBO and TSC4X solutions were mixed up at different concentration rations (10:0, 9:1, 8:2, 7:3, and so on) and the total molar concentration of ([RIBO]+[TSC4X]) was kept constant. The mole fraction of the vitamin RIBO {R = [RIBO]/([RIBO]+[TSC4X])} was in the range of 0−1 (Table S2), and the absorbance values of all the experimental solutions were measured at λ_{max} = 446 nm for the vitamin RIBO at the temperature of 298.15 K. Thereafter, to obtain Job's plot, $\Delta A \times R$ was plotted against R; here, ΔA denotes the difference of absorbance of RIBO in the absence and presence of TSC4X and R = [RIBO]/([RIBO]+[TSC4X]). The stoichiometry of RIBO-TSC4X complexation in aqueous solution was determined by the R values with the highest deviation point, that is, in many published articles, it is mentioned that the value of R is 0.5 for the 1:1 RIBO: TSC4X complex, R is 0.66 for the 2:1 complex, and R is 0.33 for the 1:2 complex.[43] In our current work, it has been viewed from Figure 1a that the highest deviation point at R = 0.5, suggesting the formation of an inclusion complex between RIBO and TSC4X with a 1:1 stoichiometric ratio.

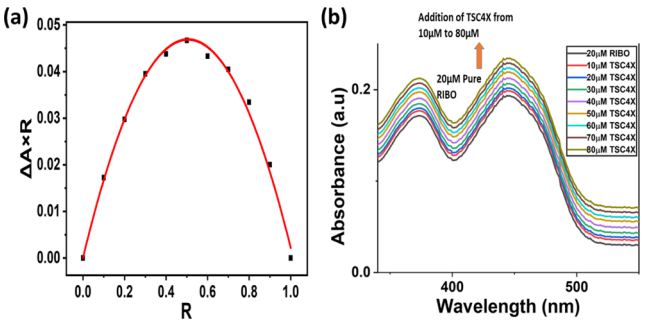

Figure 1. (**a**) Job's plot spectra for the RIBO-TSC4X complex at λ_{max} = 446 nm and (**b**) UV−vis spectra of RIBO with varying concentrations of TSC4X.

3.2. Determination of Association Constant (K_a) Using Benesi-Hildebrand Method. The characteristic change in molar absorbance of the pure RIBO was noticed when it was inserted into the hollow cavity of TSC4X.[44] The stability constant or association constant of RIBO-TSC4X complexation was determined based on the change in absorbance of RIBO using UV−vis spectroscopy. The encapsulation of RIBO molecules into the TSC4X cavity results in the steady increase of the absorbance of RIBO (Figure 1b). The occurrence of such a hyperchromic shift is attributed to the decrease in polarity of the environment of TSC4X cavity encountered by the RIBO molecules during the formation of the encapsulated complex. The value of K_a was calculated by examining the change in the absorbance of RIBO (λ_{max} = 446 nm) as a function of TSC4X concentration at 298.15 K. A well-established Benesi-Hildebrand method was utilized to produce a double reciprocal plot for a 1:1 host−guest complex using the following equation[45] (Figure S1)

$$\frac{1}{\Delta A} = \frac{1}{\Delta\varepsilon[\mathbf{RIBO}]k_a}\frac{1}{[\mathbf{TSC4X}]} + \frac{1}{\Delta\varepsilon[\mathbf{RIBO}]} \quad (2)$$

https://doi.org/10.1021/acsomega.2c07396
ACS Omega 2023, 8, 6778−6790

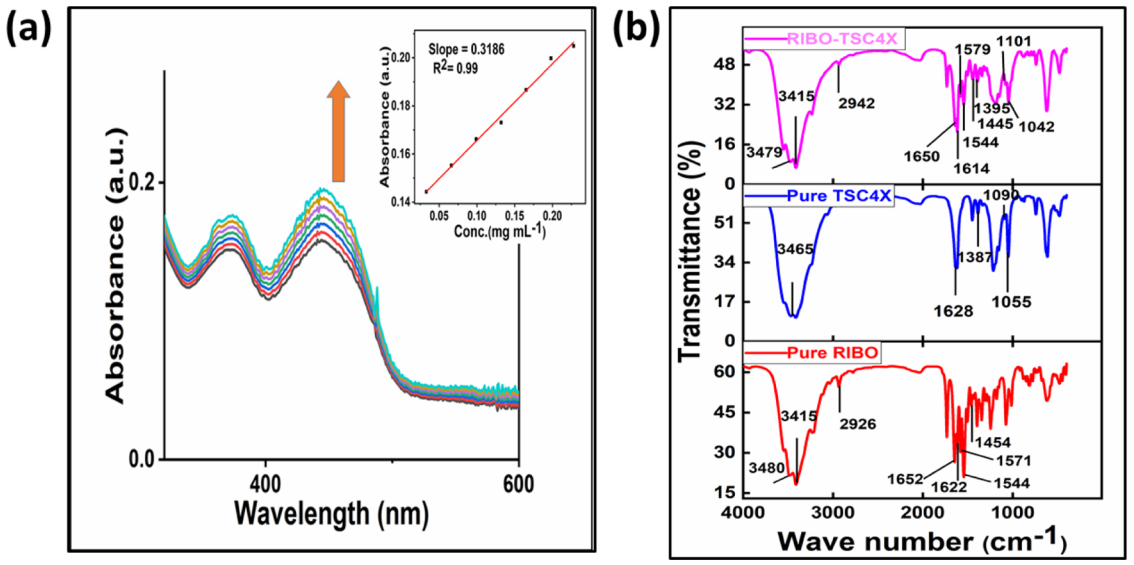

Figure 2. (a) Absorption spectra of the RIBO-TSC4X complex at different concentrations (mg mL^{-1}) in aqueous solution at 25 °C, (b) FT-IR spectra of pure RIBO, TSC4X, and RIBO-TSC4X complex.

where $\Delta\varepsilon$ represents the difference in molar extinction coefficient of RIBO without and with TSC4X, and [RIBO] is the molar concentration of RIBO. The value of molecular association constant (K_a) of the RIBO-TSC4X complex was achieved by intercept/slope ratio of the straight line of the double reciprocal plot using eq 2, and the obtained value of K_a for the RIBO-TSC4X complex was 3116.29 ± 0.17 M^{-1} at 298.15 K (Table S3). Using the value of K_a, we can easily calculate the free energy change (ΔG) due to encapsulation process by the following eq 3, and it was found to be −4.74 Kcal mol^{-1} (Table S4).

$$\Delta G^0 = -RT \ln K_a \quad (3)$$

The negative value of ΔG indicates that the formation of the RIBO-TSC4X complex is thermodynamically feasible. This result is due to the presence of hydrogen bonding and van der Waals interactions in the encapsulated complex.

3.3. Aqueous Solubility Test. UV−vis spectroscopy was used to measure the aqueous solubility of the RIBO-TSC4X complex and that was compared with the literature value for pure RIBO.[46] Figure 2a shows the UV−vis spectra of aqueous RIBO-TSC4X complex at 25 °C. Initially, the aqueous solubility of pure RIBO was very low due to its poor solubility in water but when RIBO is complexed with TSC4X, its solubility was increased remarkably.[47] The absorbance value of the solutions was measured at λ_{max} = 446 nm, as shown in Figure 2a. The peak intensity gets increased with the increase in concentration of RIBO-TSC4X complex but no change in the peak position was observed. A straight line was obtained by plotting absorbance versus concentration of RIBO-TSC4X at 446 nm as displayed in Figure 2a. The absorption coefficient of RIBO-TSC4X complex in water was found to be 0.3186 mL·mg^{-1}·cm^{-1} (at 25 °C) using Lambert−Beer's law. The absorbance value of 1.205 was obtained for the saturated solution of RIBO-TSC4X inclusion complex (Figure S2). Table S5 shows the aqueous solubility data of pure RIBO and RIBO-TSC4X complex at 25 °C. Thus, by comparing the solubility data given in Table S5, it is evident that the RIBO-TSC4X complex has a solubility of 3.78 ± 0.13 mg·mL^{-1} which is almost 30 times greater than that of pure RIBO of 0.10−0.13 mg·mL^{-1} only in the aqueous medium.[48] Hence, we can easily conclude that the formation of the RIBO-TSC4X complex enhances the solubility of RIBO to a greater extent compared to pure RIBO. Basically, the host molecule TSC4X which is sufficiently soluble in water has played a significant role to improve the aqueous solubility of RIBO due to the formation of the RIBO-TSC4X complex.

3.4. FT-IR Spectral Analysis. Among several important characterization tools, one of the most important and authentic methods to study the development of a new RIBO-TSC4X complex is FT-IR spectral analysis.[49] The creation of a new complex from pure RIBO and TSC4X may involve different interactions such as hydrophobic, H-bonding, Van der Waals interaction, and so forth.[50]

The pure RIBO displayed an absorption band at 3480 cm^{-1} for the O−H group, and the decrease in stretching frequency of O−H from its typical value may be due to the intramolecular H-bonding among the O−H groups in the ribityl side chain {$-CH_2-CH(OH)-CH(OH)-CH(OH)-CH_2OH$} and the N−H bond stretching frequency viewed at 3415 cm^{-1}. The C−H stretching band was observed at 2926 cm^{-1}, C−H bending from $-CH_3$ appeared at 1454 cm^{-1}, and the aromatic C═C stretching band at 1622, 1571, and 1544 cm^{-1}, whereas the carbonyl (C═0) stretching frequency in the imide group (−CO−NH−CO−) was observed at 1652 cm^{-1} (Figure 2b).

On the other hand, pure TSC4X showed characteristic stretching frequency at 3465 cm^{-1} for the aromatic O−H group, $-SO_3H$ stretching vibration at 1090 and 1055 cm^{-1}. The aromatic C═C stretching band appeared at 1628 cm^{-1} and Ar−H bending vibration at 1387 cm^{-1}.[51]

After encapsulation of RIBO with TSC4X, a certain shift in stretching vibration was observed for both RIBO and TSC4X. Meanwhile, the stretching bands for O−H (3479 cm^{-1}), N−H (3415 cm^{-1}), and C═0 (1650 cm^{-1}) remained almost unaffected. The C−H stretching and C−H bending from the $-CH_3$ group appeared at 2926 and 1454 cm^{-1}, respectively, in pure RIBO and got shifted to 2942 cm^{-1} and 1445, respectively, in the RIBO-TSC4X complex. Therefore, it can be suggested that two $-CH_3$ groups attached to C-7 and C-8

https://doi.org/10.1021/acsomega.2c07396
ACS Omega 2023, 8, 6778−6790

Scheme 1. 2D Structures of (a) RIBO and (b) *p*-Sulfonatothiacalix[4]arene

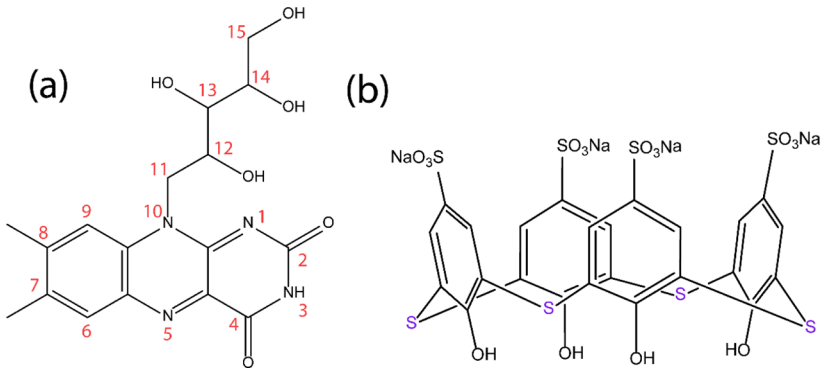

carbon atoms of the aromatic ring of RIBO have been incorporated into the TSC4X cavity. It is worth mentioning that the aromatic C═C stretching frequency viewed at 1622, 1571, and 1544 cm^{-1} for pure RIBO also moved to new stretching bands at about 1614,1579, and 1544 cm^{-1} in the complex (Figure 2b). The $-SO_3H$ stretching band observed at 1090 and 1055 cm^{-1} in pure TSC4X have also been moved to 1101 and 1042 cm^{-1}, respectively, in the encapsulated complex. The Ar−H bending vibration of TSC4X at 1387 cm^{-1} also changed to 1395 cm^{-1} in the complex. Hence, it can be concluded that, the ring bearing two C═O groups and −NH and also the ribityl side chain {$-CH_2-CH(OH)-CH(OH)-CH(OH)-CH_2OH$} have not been incorporated into the TSC4X cavity after complexation. It is only two $-CH_3$ groups attached to C-7 and C-8 atoms of the aromatic moiety of RIBO have been inserted into the cavity of TSC4X, as also evident from the molecular docking study (Figure 5).

3.5. ^{1}H-NMR Examination. ^{1}H-NMR spectroscopy is a useful technique that can be utilized to explore the possible binding mode of RIBO with TSC4X by analyzing the changes in chemical shift values ($\Delta\ \delta$) of both RIBO and TSC4X protons.[52] The ^{1}H-NMR spectra of pure RIBO, TSC4X, and RIBO-TSC4X complex in D_2O solvent are shown in Figure S3, and the corresponding chemical shift values (δ) of their protons are summarized in Table S7.

After the complexation of pure RIBO with TSC4X, two −CH3 groups attached to C-7 and C-8 carbon atoms of RIBO undergo upfield chemical shift having $\Delta\delta$: −0.03 and −0.02 ppm, respectively, whereas protons such as H-6, H-9, H-11, H-12, H-13, H-14, and H-15 undergo zero or downfield chemical shift change ($\Delta\delta$), as shown in Table S7.

On the other hand, ^{1}H-NMR spectra of pure TSC4X revealed that it has two peaks in ^{1}H-NMR spectra for Ar−H and Ar−OH protons and the corresponding chemical shift values are 7.95 ppm and 3.44−3.42 ppm, respectively.[53] However, after complexation, the Ar−H proton undergoes an upfield change in the chemical shift value with $\Delta\delta$ = −0.04 ppm, whereas the Ar−OH proton undergoes slightly downfield chemical shift change having $\Delta\delta$ = 0.02 ppm.

Based on the above ^{1}H-NMR results, it is almost confirmed that two −CH3 groups attached to C-7 and C-8 carbon atoms of the aromatic moiety of RIBO got incorporated into the hydrophobic cavity of TSC4X. The Π−Π stacking, hydrophobic, and electrostatic interactions act as the driving force to provide stability to the complex. The possible binding mode of RIBO with TSC4X as received from the ^{1}H-NMR analysis is given in Scheme 2.

Scheme 2. Possible Binding Orientation of the RIBO-TSC4X Complex Using ^{1}H-NMR

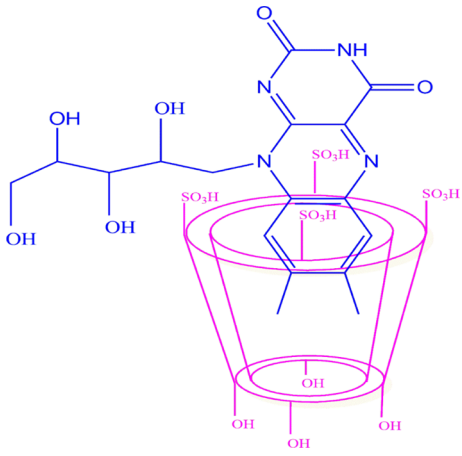

3.6. PXRD Analysis. PXRD spectral analysis offers substantial evidence in favor of the formation of RIBO-TSC4X encapsulated complex derived from pure RIBO and TSC4X.[54] The individual characteristic diffraction pattern of RIBO and TSC4X was found to be altered after complexation. The construction of a new solid encapsulated complex of RIBO-TSC4X can be confirmed by comparing the diffraction outlines of the pure compounds with their corresponding complex.[55] From Figure 3a, it has been detected that both RIBO and TSC4X showed sharp and relatively higher intense peaks compared to that of the solid RIBO-TSC4X complex. The sharp and distinct peaks viewed for pure RIBO at 10.24, 11.43, 14.28, 17.35, 19.51, 21.64, and 29.73° confirm the crystalline nature of it, whereas pure TSC4X displayed characteristic diffraction patterns at angles of 10.12, 12.85, 15.70, 16.18, 19.27, 21.88, 25.21, 26.88, 31.15, and 33.30°. These peaks are also sharp in nature and assure its crystallinity.

On the other hand, RIBO after complexation with TSC4X (RIBO-TSC4X complex) validates different diffraction patterns and the relocation or disappearance of some peaks have also been examined. For the RIBO-TSC4X complex, the observed peaks are 9.06, 10.48, 11.67, 12.61, 14.28, 17.61, 19.51, 20.70, 22.12, 25.91, and 30.21°.

Therefore, the manifestation of new peaks with less intensity and vanishing of some peaks in the solid complex ascertains the development of the RIBO-TSC4X complex.

3.7. SEM Examination. The surface character, morphology, and particle size of solid samples were precisely examined by SEM analysis.[56] The encapsulation of RIBO with TSC4X

https://doi.org/10.1021/acsomega.2c07396
ACS Omega 2023, 8, 6778−6790

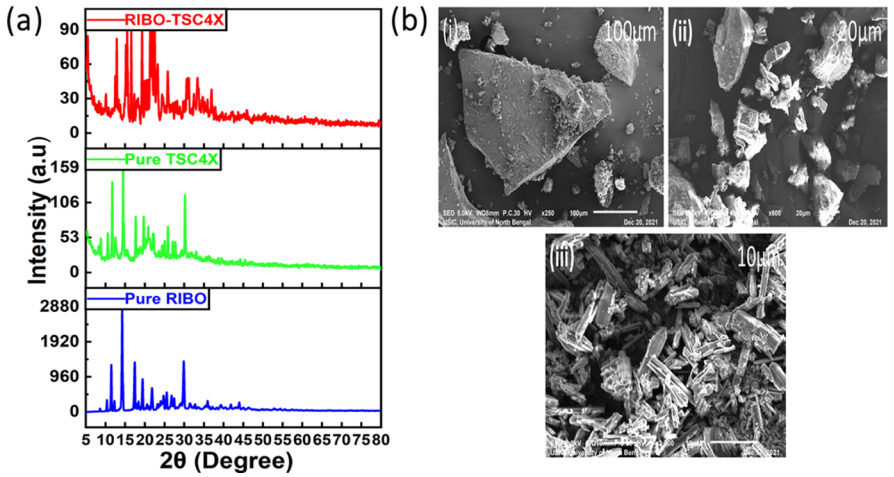

Figure 3. (a) Powder XRD plots; (b) SEM images of (i) pure RIBO, (II) pure TSC4X, and (III) RIBO-TSC4X complex.

leads to having different surface morphologies compared to pure RIBO & Pure TSC4X compounds. The SEM micro images of pure RIBO, TSC4X, and RIBO-TSC4X complex are shown in Figure 3b. Thus, from Figure 3b, it has been noticed that pure RIBO has an uneven cubic-type structure, whereas TSC4X has parallelogram-like shaped particles. However, when RIBO and TSC4X are complexed, the surface morphology gets changed to a mixture of rectangular and needle-shaped crystals. The surface nature of the RIBO-TSC4X complex is different from that of pure RIBO and TSC4X, which gives an adequate mark in favor of the formation of the complex.

3.8. TGA Investigation. The thermal stability of RIBO after its encapsulation into the TSC4X cavity was examined using TG analysis. The encapsulation of RIBO into the TSC4X cavity may result in change of the melting point, boiling point, or sublimation point to another temperature or vanishes. Figure 4 displayed the TGA curve of pure RIBO, TSC4X, and

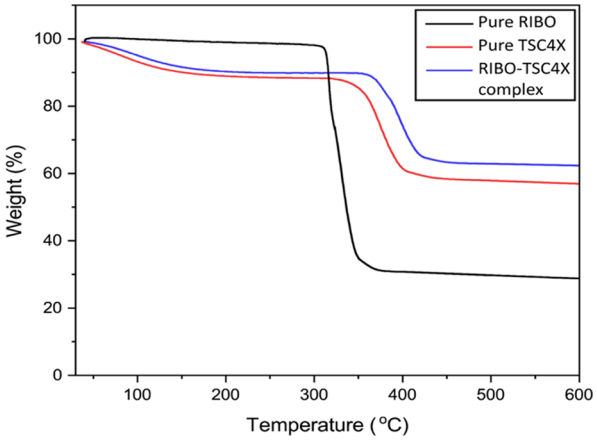

Figure 4. TGA thermograms of pure RIBO, TSC4X, and RIBO-TSC4X complex.

RIBO-TSC4X encapsulated complex. The TGA curves demonstrate that no weight loss for pure RIBO was noticed below 150 °C, which confirms the absence of moisture in it. During the thermal decomposition of RIBO, it furnishes weight loss at a temperature ranging from 268 to 380 °C. Here, the thermal decomposition mainly occurs at the RIBO block with the formation of alcohol, ethylene, and acetaldehyde.[57]

Whereas, both TSC4X and RIBO-TSC4X complexes presented two phases of mass loss temperature. The first phase of degradation for TSC4X and the complex has occurred at the same temperature range of 64−95 °C due to H_2O loss from the respective molecules. However, the second phase of decomposition of pure TSC4X occurred at the temperature range 270−410 °C and that for the complex took place in the range 320−440 °C.[58] Therefore, based on the above argument, we can summarize that the RIBO-TSC4X complex decomposes at a higher range of temperature compared to pure RIBO, leading to the greater thermal stability of the former than that of the latter.

3.9. Molecular Modeling. Molecular docking helps us to predict the possible bound conformation of the RIBO-TSC4X encapsulated complex and to estimate the binding affinity in the gas phase.[59] Figure 5 shows the binding mode observed in

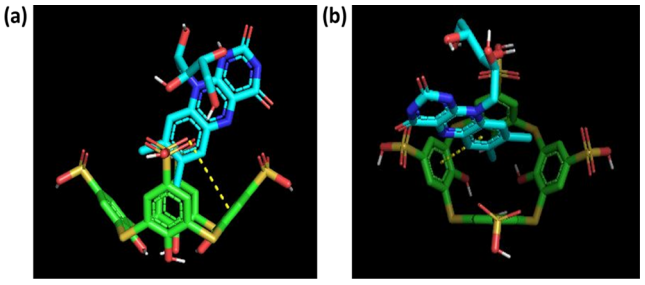

Figure 5. Docked orientation images of RIBO-TSC4X complex: (a) side view; (b) top view.

two different ways (top view and side view) with respect to TSC4X. The experimental results showed that the formation of the RIBO-TSC4X complex is a 1:1 ratio with respect to the guest and host having a binding affinity of −4.1 Kcal/mole, as negative binding energy indicates a stable inclusion complex which is in good agreement with the experimental outcomes from UV−visible spectroscopy. The results also showed that only two methyl groups ($-CH_3$ groups) attached to C-7 and C-8 carbon atoms of the aromatic moiety of RIBO (Schemes 1 and 2) got incorporated into the cavity of TSC4X and stabilized by Π−Π stacking and hydrophobic interactions. Whereas, the ribityl side chain was located outside of the TSC4X cavity. The binding conformation obtained from the

https://doi.org/10.1021/acsomega.2c07396
ACS Omega 2023, 8, 6778−6790

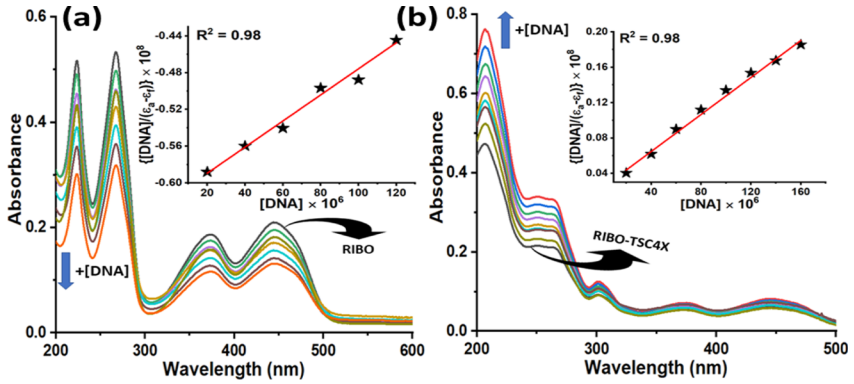

Figure 6. Change in UV−vis spectra of (**a**) RIBO and (**b**) RIBO-TSC4X with incremental addition of CT-DNA. Inset: Wolfe−Shimer plot for the calculation of K_b.

molecular docking study is also supported by the results of FT-IR and ^{1}H-NMR experiments.

3.10. DNA Interaction Studies by UV−Vis Titration. UV−vis spectroscopic titration is a widely used technique for the determination of binding affinity and mode of binding of small molecule with DNA. With the increase in the concentration of CT-DNA, the change in absorbance of RIBO or RIBO-TSC4X was monitored. It is found that the hypochromic shift is observed in the case of UV-titration of RIBO with CT-DNA (Figure 6a). This suggests that RIBO stabilizes the secondary structure of DNA by intercalation.[60] The UV−vis spectra of RIBO-TSC4X show a hyperchromic shift (Figure 6b), indicating destabilization of the secondary structure by groove binding.[61] Wolfe−Shimer eq 4 was employed for the calculation of the binding constant.[62]

$$\frac{[\mathrm{DNA}]}{\varepsilon_a - \varepsilon_f} = \frac{[\mathrm{DNA}]}{\varepsilon_b - \varepsilon_f} - \frac{1}{K_b(\varepsilon_b - \varepsilon_f)} \quad (4)$$

Here, the concentration of CT-DNA is denoted by [DNA], ε_a is given by $A_{obs}/[C]$, where A_{obs} is the absorbance and [C] is the concentration of RIBO or RIBO-TCS4X, ε_b represents the extinction coefficient of free RIBO or RIBO-TCS4X, and ε_f indicates the extinction coefficient when the RIBO or RIBO-TCS4X fully bound with CT-DNA. K_b is the binding constant which is determined from the slope to intercept ratio of the Wolfe−Shimer plot ($[\mathrm{DNA}]/(\varepsilon_a-\varepsilon_f)$ vs [DNA]). The calculated K_b values are presented in Table 1 which are

Table 1. K_b and ΔG Values for the DNA-Complex Interaction

compound	K_b (M^{-1}) × 10^{-4}	ΔG (kJ mol^{-1})
RIBO	0.34 ± 0.01	20.15
RIBO-TSC4X	0.23 ± 0.02	19.18

more or less similar, suggesting that the DNA binding affinity of RIBO is not changed significantly after the formation of the inclusion complex. The free energy changes due to binding interaction were calculated by the following eq 5

$$\Delta G = -RT \ln K_b,\ T = 298.15\ \mathrm{K} \quad (5)$$

The calculated ΔG is negative indicate DNA binding occurs spontaneously.

3.11. BSA Binding Studies by UV−Vis Spectroscopic Method. For drug transportation and drug delivery, serum albumin (SA) plays a key role in human body. Due to structural homology with human SA (HSA), BSA is used as a model protein for the interaction with the drug molecule (RIBO) and the inclusion complex (RIBO-TSC4X). The peak at 280 nm is mainly due to the tryptophan and tyrosine residues present[63] in BSA which increase with an increase in the concentration of drug molecule or inclusion complex (Figure 7a,b). Thus, the increase in absorbance at 280 nm suggests both the drug molecule and inclusion complex change the microenvironment near tryptophan or tyrosine residues. The spectral change by the addition of RIBO and RIBO-TCS4X was further analyzed[64] by following eq 6.

$$\frac{1}{(A - A_0)} = \frac{1}{(A_\infty - A_0)} + \frac{1}{[C]} \times \frac{1}{K_b(A_\infty - A_0)} \quad (6)$$

where A_0 and A are the absorbance of BSA at 280 nm in the absence and presence of interacting complex (RIBO or RIBO-TCS4X). A_∞ is the absorbance of BSA when the compound is fully bound. K_b is binding constant which is calculated from the intercept to slope ratio of $1/(A-A_0)$ versus $1/[C]$ plot. The calculated K_b values of RIBO and RIBO-TCS4X are 0.26×10^4 and 0.21×10^4 M^{-1}, respectively, which are very close. Thus, BSA binding ability does not change significantly after the formation of inclusion complex. The binding constant is also suitable for their carrier activity in blood plasma.

3.12. Antioxidant and Metal Chelation Activity. Oxidative stress can simply be defined as an increased production of reactive oxygen species (ROS) or a reduced ability of scavengers, that is, the imbalance between generation and accumulation of ROS. Oxidative stress is one of the prime reasons for the development of many chronic diseases such as cancer, cardiovascular diseases, and diabetes. Improving the antioxidant potential may be a way out in the reduction of oxidative stress. Nutrients such as vitamins C and E and carotenoids are reported to have antioxidant capability. However, the role of RIBO as an antioxidant nutrient is somehow neglected, but this particular vitamin plays an antioxidant action independently or as a constituent of the glutathione redox cycle. A thorough review was done on RIBO and its antioxidant capability and came up with two main aspects of RIBO viz. prevention of lipid peroxidation and attenuation of reperfusion oxidative injury.[65]

Antioxidant activity of the formed RIBO-TSC4X complex and guest molecule RIBO was expressed in terms of IC_{50} value, and the collected data are displayed in Table 2. The IC_{50} value of the synthesized inclusion complex was found to be lower than that of the guest molecule RIBO, where a low IC_{50} value

https://doi.org/10.1021/acsomega.2c07396
ACS Omega 2023, 8, 6778−6790

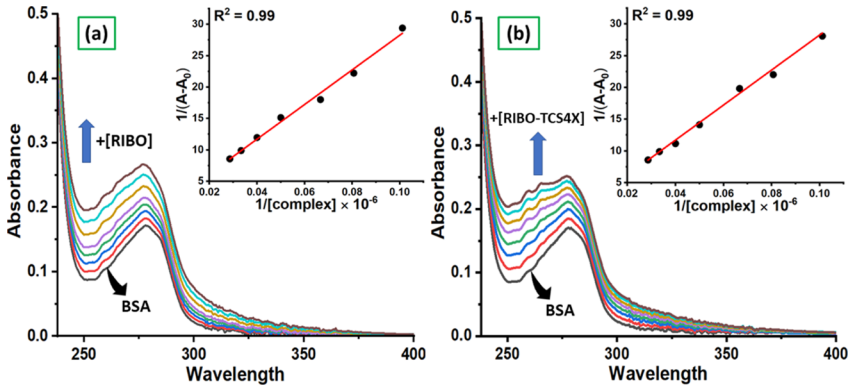

Figure 7. Change in absorption spectra of BSA (10 μM) with the increase in concentration of (**a**) RIBO and (**b**) RIBO-TCS4X (0−35 μM).

Table 2. ABTS, DPPH, Super Oxide Scavenging, FRAP, and Metal Chelation Activity of RIBO-TSC4X in Comparison to Pure RIBO (Results Were Presented as Mean ± Standard Deviation of Three Replications)

	antioxidant activity (IC50 value in mM/mL)				FRAP
sample name	ABTS	DPPH	SUPEROXIDE	METAL CHELATION	μg AAE/mM compound
RIBO	2.867 ± 0.051	3.177 ± 0.042	2.783 ± 0.070	12.853 ± 0.102	14.133 ± 0.231
RIBO-TSC4X	2.043 ± 0.031	2.823 ± 0.103	2.173 ± 0.047	7.887 ± 0.080	19.867 ± 0.282

denotes a high level of antioxidant activity. DPPH radical scavenging assay is the simplest type of antioxidant test which requires less time, a low amount of reagent, and a test sample.[66] From the results it was observed that synthesized inclusion complex at 1.75 mM/mL dosage exhibited 33.49% inhibition against the DPPH radical which is 20.94% is higher than the RIBO itself (Figure 8). The blue chromophore

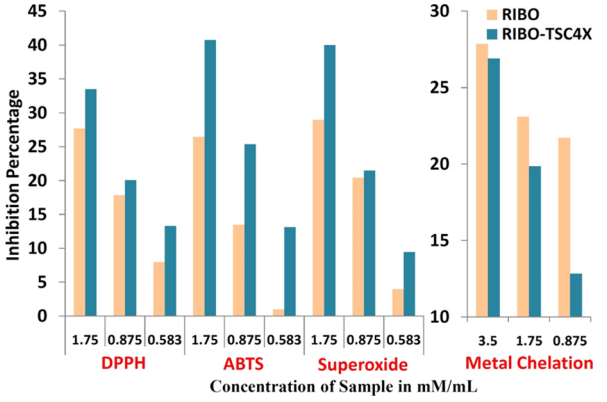

Figure 8. Inhibition percentage showed by studied samples against the tested free radicals.

$ABTS^+$, which is formed through the oxidation of ABTS by potassium persulfate, creates oxidative damage. Findings of the current study demonstrated that after inclusion within *p*-sulfonatothiacalix[4]arene (TSC4X), RIBO showed 41.16% higher $ABTS^+$ radical scavenging activity. Superoxide is another detrimental free radical which alleviates hydroxyl radical formation and consequent DNA damage in cells. Some other hypothesis suggested that superoxide increase oxidative damage by discharging iron from ferritin. Furthermore, superoxide caused iron overload by leaching from iron sulfur (4Fe−4S) enzymic clusters and storage proteins.[67] Free iron deposits on the DNA surface and forms DNA-oxidants in association with other electron donors, thereby causing DNA damage. RIBO after encapsulation with TSC4X exhibited a lower IC_{50} value as experienced through superoxide radical scavenging assay and metal chelation activity. FRAP assay which measures the reducing potential (Fe^{+3} to Fe^{+2}) of a sample demonstrated that the prepared inclusion complex had better activity than RIBO alone. On summarizing overall results, it can be concluded that biosynthesized RIBO-TSC4X showed maximum activity against $ABTS^+$ radical and least for metal chelation activity. The observed antioxidant activity of the RIBO-TSC4X host−guest complex could be attributed to various mechanisms including prevention of chain initiation, prevention of continued hydrogen abstraction, decomposition of peroxides and binding of transition metal ion catalysts.[68] The properties of the TSC4X that remain bound with the synthesized inclusion complex might be the reason for improved antioxidant activity. This alleviating action might be due to the increased solubility of the RIBO-TSC4X complex (30 times higher than pure RIBO) as observed through spectrophotometric analysis. Many researchers suggested that drug having poor aqueous solubility generally have low absorption rate which leads to inadequate and variable bioavailability that eventually render the drug ineffective. In contrast, high solubility makes a drug or medicine highly available at the site of action which increases the effectiveness of a drug.

3.13. Anti-Lipid Peroxidation Capability of RIBO-TSC4X. The lipid peroxidation protection capability of RIBO and the RIBO-TSC4X complex was evaluated using the rat liver homogenate. Experimental results suggested that the synthesized RIBO-TSC4X inclusion complex provides better inhibition potentiality against the lipid peroxidation in comparison to pure RIBO. At 7 mM/mL concentration, the studied RIBO-TSC4X demonstrated 77.55 percent inhibition against lipid peroxidation (generated in rat liver exposed to oxidation medium) which is 2.89% higher than the RIBO (Figure 9). Obtained inhibition percentage was concentration-dependent and showed IC_{50} values of 1.04 and 0.17 mM/mL for RIBO and RIBO-TSC4X complex, respectively.

3.14. Peroxidase-like Activity and Steady State Kinetics. TSC4X catalyzes many oxidation−reduction reac-

https://doi.org/10.1021/acsomega.2c07396
ACS Omega 2023, 8, 6778−6790

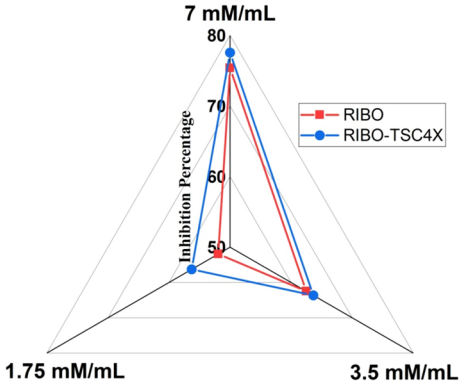

Figure 9. Radar plot representing the inhibition percentage of the studied samples against lipid peroxidation.

tions, and inspired by the fact, we introduced the RIBO-TSC4X complex (IC) to catalyze some biological reactions. Figure 10a showed that pure TSC4X could not catalyze the oxidation of TMB but the introduction of a small amount of H_2O_2 leads to efficient oxidation of TMB, resulting in the formation of blue colored TMBox which gives a characteristic absorption peak at 652 nm. The above experiment indicated that the TSC4X catalyzed only the peroxidase reaction but not the oxidase reaction. On inclusion of RIBO into TSC4X could trigger the oxidation reaction and achieve high absorbance with same amount of catalyst. In contrast, RIBO could not catalyze the oxidation of TMB, indicating that peroxidase activity shown by RIBO-TSC4X complex has only come from TSC4X (Figure 10b). The peroxidase reaction is time- and pH-dependent. Figure 10c showed the time-dependent plot, the absorbance increased with time and achieved a maximum at 30 min and then remain constant, which means 30 min incubation period is the optimum time for the present peroxidase system. Peroxidase reaction is highly pH-dependent, and most of the artificial peroxidase enzyme is active in an acidic medium; here, the high absorbance achieved at pH-3 and the absorbance gradually decreases upon increasing or decreasing the pH shown in Figure 10d.

The oxidation reaction catalyzed by the RIBO-TSC4X complex follows the typical Michaelis–Menten behavior toward substrates H_2O_2 (Figure 10e). The important kinetics parameter obtained from the Line Weaver–Burk plot (Figure 10f). Typical K_m = 13.9 and V_{max} = 1.77 μM/min are obtained from linear rigration R^2 = 0.99245. The obtained K_m value for H_2O_2 is lower than some other earlier reports shown in Table 3, which indicates the present system might be become an important catalyst in bioanalytical applications.

4. CONCLUSIONS

In our study, we have successfully synthesized the novel RIBO-TSC4X complex using the co-precipitation method. The

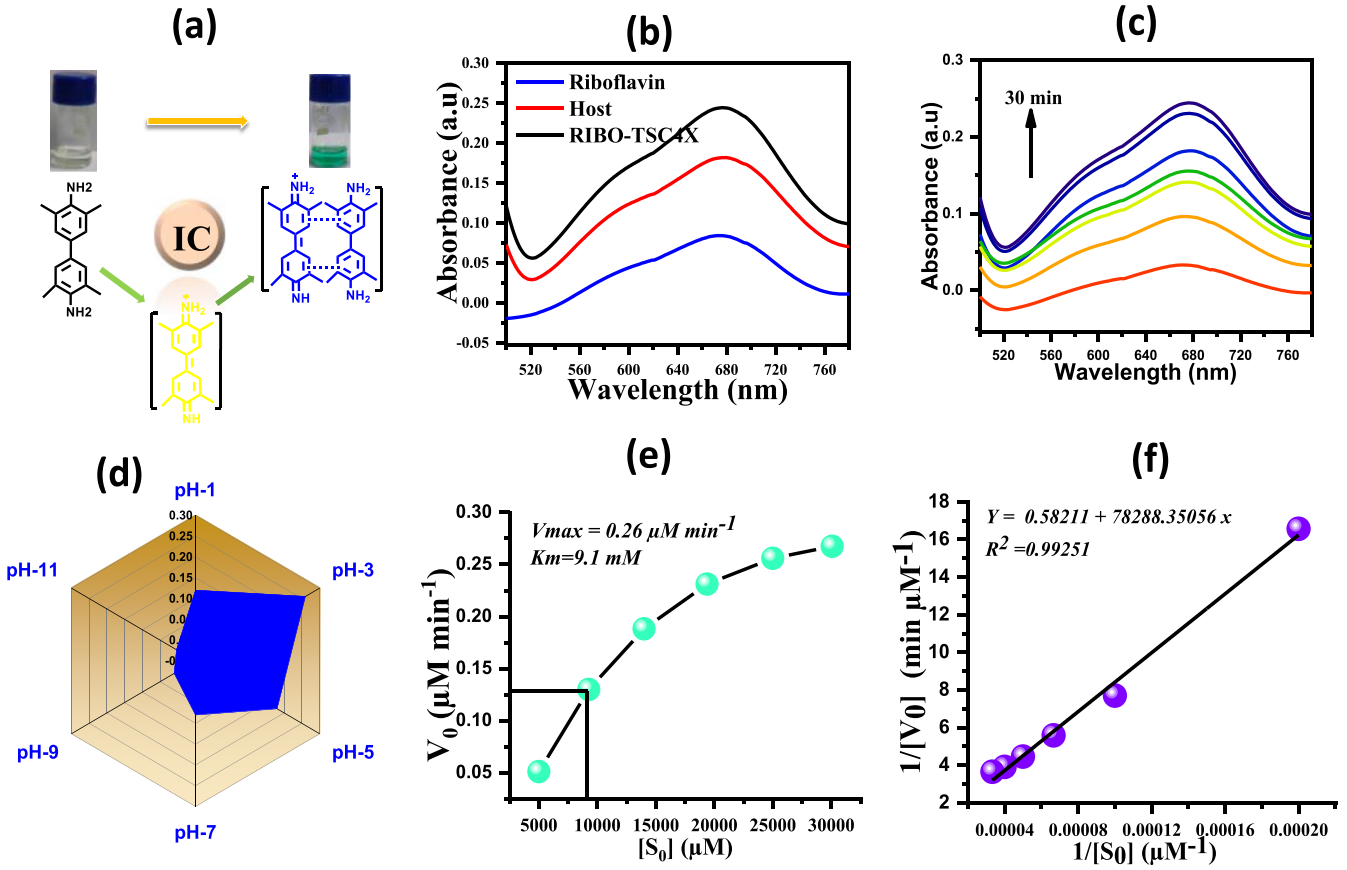

Figure 10. (a) Diagrammatic representation of peroxidase- and oxidase-like activity of RIBO-TSC4X complex (IC) with TMB. Absorbance by different systems TMB (380 μM) + H_2O_2 (20 mM) (b). Time-dependent absorbance by different systems TMB (380 μM) + H_2O_2 (20 mM) and IC (250 μM) (c) vs different conditions in same time. Absorbance of TMB (380 μM) + IC (250 μM) + H_2O_2 (20 mM) system in different pH values (d). Steady state kinetic analysis of IC as peroxidase mimetic: (e) curve of velocity against the H_2O_2 concentration in conditions of 380 μ M TMB, room temperature, pH 5. (f) Double-reciprocal plots of (e).

https://doi.org/10.1021/acsomega.2c07396
ACS Omega 2023, 8, 6778−6790

Table 3. Kinetics Parameters K_m and V_{max} of TMB and H_2O_2 Compared with the HRP and Other Nano Enzymes

system	substrate	K_m	V_{max}	reference
β-CD grafted R−CuO NPs	H_2O_2	5.4238	20.324×10^{-6}	69
Fe3O4 MNPs	H_2O_2	154	78×10^{-8}	70
RIBO-TSC4X (IC)	H_2O_2	13.934	1.77×10^{-6}	Present work

prepared complex was then characterized by spectroscopic methods such as ^{1}H-NMR, FT-IR, TGA, PXRD, and SEM analysis. From FT-IR spectral examination, it was predicted that two $-CH_3$ groups attached to C-7 and C-8 carbon atoms of the aromatic moiety of RIBO got incorporated into the hydrophobic cavity of TSC4X, which was further confirmed by the ^{1}H-NMR investigation. Job's plot confirms the insertion of RIBO into TSC4X cavity with a 1:1 molar ratio. Furthermore, the extent of stability of the RIBO-TSC4X complex was determined by assessing the association constant (K_a) value, which was found to be 3116.29 ± 0.17 M^{-1}. The most stable binding orientation between RIBO and TSC4X was visualized by molecular docking study, which also revealed that two methyl groups attached to C-7 and C-8 carbon atoms of RIBO got inserted into the TSC4X cavity as already confirmed by experimental analysis (FT-IR and ^{1}H-NMR). The increment in aqueous solubility of the RIBO-TSC4X complex compared to pure RIBO was investigated using a UV−vis spectrophotometer and result demonstrates that former (complex) has almost 30 times greater solubility than the latter (pure RIBO). The enrichment of thermal stability of RIBO upto 440 °C after complexation with TSC4X was examined by TG analysis. This research also forecasts RIBO's release behavior in the presence of CT-DNA, and at the same time, BSA binding study was also carried out. The encapsulation of RIBO with TSC4X sufficiently improves the antioxidant activity of pure RIBO. This finding will be helpful in the medicinal chemistry and pharmaceutical industry to design a new type of vitamin added antioxidant nutrient. Moreover, the synthesized RIBO-TSC4X complex showed biomimetic catalytic activities such as POD-like activity.

■ ASSOCIATED CONTENT

Supporting Information

The Supporting Information is available free of charge at https://pubs.acs.org/doi/10.1021/acsomega.2c07396.

Detailed descriptions of all the chemicals used, data for Job's plot, association constant, ^{1}H-NMR spectra, FT-IR spectra, aqueous solubility, double reciprocal plot, and UV spectra (PDF)

■ AUTHOR INFORMATION

Corresponding Author

Mahendra Nath Roy − *Department of Chemistry, University of North Bengal, Darjeeling 734013 West Bengal, India;* orcid.org/0000-0002-7380-5526; Email: mahedraroy2002@yahoo.co.in

Authors

Biswajit Ghosh − *Department of Chemistry, University of North Bengal, Darjeeling 734013 West Bengal, India*

Niloy Roy − *Department of Chemistry, University of North Bengal, Darjeeling 734013 West Bengal, India*

Saikat Mandal − *Department of Chemistry, National Institute of Technology, Durgapur 713209, India;* orcid.org/0000-0002-2854-1015

Salim Ali − *Department of Chemistry, University of North Bengal, Darjeeling 734013 West Bengal, India*

Pranish Bomzan − *Department of Chemistry, Gorubathan Government College, Kalimpong 735231, India*

Debadrita Roy − *Department of Chemistry, University of North Bengal, Darjeeling 734013 West Bengal, India*

Md Salman Haydar − *Department of Botany, University of North Bengal, Darjeeling 734013, India;* orcid.org/0000-0003-4725-8562

Vikas Kumar Dakua − *Department of Chemistry, Alipurduar University, Alipurduar 736122 West Bengal, India*

Anupam Upadhyay − *Department of Chemistry, Alipurduar University, Alipurduar 736122 West Bengal, India*

Debabrata Biswas − *Department of Chemistry, Alipurduar University, Alipurduar 736122 West Bengal, India*

Kausik Kumar Paul − *Department of Chemistry, Alipurduar University, Alipurduar 736122 West Bengal, India*

Complete contact information is available at: https://pubs.acs.org/10.1021/acsomega.2c07396

Notes

The authors declare no competing financial interest.

■ ACKNOWLEDGMENTS

The authors are extremely happy to acknowledge SAP, Department of Chemistry, North Bengal University under UGC, New Delhi for providing instruments to complete the research work. Corresponding author Prof. (Dr) M.N. Roy is highly thankful to UGC for being awarded grant from UGC-BSR. B. Ghosh acknowledges CSIR for Junior Research fellowship {Ref. no. 17/12/2017(ii) EUV}. The authors are also thankful to Cochin University, SAIF for analytical instrumentation facility including TGA, DSC, and PXRD and Panjab University, CIL for FT-IR analysis. All the authors acknowledge Cell and Molecular Biology Laboratory, University of North Bengal for providing fresh liver samples of Wistar albino rats.

■ REFERENCES

(1) Thakur, K.; Tomar, S. K.; Singh, A. K.; Mandal, S.; Arora, S. Riboflavin and health: a review of recent human research. *Crit.Rev.Food.Sci.Nutr.* **2017**, *57*, 3650−3660.

(2) Averianova, L. A.; Balabanova, L. A.; Son, O. M.; Podvolotskaya, A. B.; Tekutyeva, L. A. Production of vitamin B2 (riboflavin) by microorganisms: An overview. *Front. Bioeng. Biotechnol.* **2020**, *8*, 570828.

(3) Suwannasom, N.; Kao, I.; Pruß, A.; Georgieva, R.; Bäumler, H. Riboflavin: The health benefits of a forgotten natural vitamin. *Int. J. Mol. Sci.* **2020**, *21*, 950.

(4) Choi, J. Y.; Kim, Y. N.; Cho, Y. O. Evaluation of riboflavin intakes and status of 20−64-year-old adults in South Korea. *Nutrients* **2014**, *7*, 253−264.

(5) Thakur, K.; Tomar, S. K.; De, S. Lactic acid bacteria as a cell factory for riboflavin production. *Microb. Biotechnol.* **2016**, *9*, 441−451.

(6) Auclair, O.; Han, Y.; Burgos, S. A. Consumption of Milk and Alternatives and Their Contribution to Nutrient Intakes among

Canadian Adults: Evidence from the 2015 Canadian Community Health Survey-Nutrition. *Nutrients* **2019**, *11*, 1948.
(7) Barile, M.; Giancaspero, T. A.; Leone, P.; Galluccio, M.; Indiveri, C. Riboflavin transport and metabolism in humans. *J. Inherit. Metab. Dis.* **2016**, *39*, 545−557.
(8) Couto, N.; Wood, J.; Barber, J. The role of glutathione reductase and related enzymes on cellular redox homoeostasis network. *Free Radic. Biol. Med.* **2016**, *95*, 27−42.
(9) Pinto, J. T.; Cooper, A. J. L. From Cholesterogenesis to Steroidogenesis: Role of Riboflavin and Flavoenzymes in the Biosynthesis of Vitamin D. *Adv. Nutr.* **2014**, *5*, 144−163.
(10) Udhayabanu, T.; Manole, A.; Rajeshwari, M.; Varalakshmi, P.; Houlden, H.; Ashokkumar, B. Riboflavin Responsive Mitochondrial Dysfunction in Neurodegenerative Diseases. *J. Clin. Med.* **2017**, *6*, 52.
(11) Suwannasom, N.; Kao, I.; Pruss, A.; Georgieva, R.; Baumler, H. Riboflavin: The Health Benefits of a Forgotten Natural Vitamin. *Int. J. Mol. Sci.* **2020**, *21*, 950.
(12) Lucas, T. G.; Henriques, B. J.; Gomes, C. M. Conformational analysis of the riboflavin-responsive ETF:QO-p.Pro456Leu variant associated with mild multiple acyl-CoA dehydrogenase deficiency. *Biochim. Biophys. Acta Proteins Proteom.* **2020**, *1868*, 140393.
(13) Acevedo-Rocha, C. G.; Gronenberg, L. S.; Mack, M.; Commichau, F. M.; Genee, H. J. Microbial cell factories for the sustainable manufacturing of B vitamins. *Curr. Opin Biotechnol.* **2019**, *56*, 18−29.
(14) Alam, M. M.; Iqbal, S.; Naseem, I. Ameliorative effect of riboflavin on hyperglycemia, oxidative stress and DNA damage in type-2 diabetic mice: mechanistic and therapeutic strategies. *Archi. Biochem. Biophys.* **2015**, *584*, 10−19.
(15) Ashoori, M.; Saedisomeolia, A. Riboflavin (vitamin B2) and oxidative stress: a review. *Br. J. Nutr.* **2014**, *111*, 1985−1991.
(16) Naseem, I.; Hassan, I.; Alhazza, I. M.; Chibber, S. Protective effect of riboflavin on cisplatin induced toxicities: A gender-dependent study. *J. Trace Elem. Med. Biol.* **2015**, *29*, 303−314.
(17) Mazur-Bialy, A. I.; Pochec, E.; Plytycz, B. Immunomodulatory effect of riboflavin deficiency and enrichment-reversible pathological response versus silencing of inflammatory activation. *J. Physiol. Pharmacol.* **2015**, *66*, 793−802.
(18) Bomzan, P.; Roy, N.; Ghosh, B.; Roy, M. N. Exploring inclusion complexes of amino acids with p-sulfonatothiacalix [4] arene by experimental and computational approach. *J. Mol. Str.* **2023**, *1271*, 133981.
(19) Wintgens, V.; Lorthioir, C.; Miskolczy, Z.; Amiel, C.; Biczók, L. Substituent effects on the inclusion of 1-alkyl-6-alkoxy-quinolinium in 4-sulfonatocalix [n] arenes. *ACS omega* **2018**, *3*, 8631−8637.
(20) Yamada, M.; Rajiv Gandhi, M.; Kunda, U. M. R.; Hamada, F. Thiacalixarenes: emergent supramolecules in crystal engineering and molecular recognition. *J. Incl. Phenom. Macrocycl.* **2016**, *85*, 1−18.
(21) Loh, S.; Sobolev, A. N.; Lim, S. H.; Ling, I. Influence of ortho- and meta-substituted N-heterocyclic dications towards the self-assembly of p-sulfonatocalix [4] arene. *Cryst.Eng.Comm.* **2020**, *22*, 52−60.
(22) Jing, J.; Szarpak-Jankowska, A.; Guillot, R.; Pignot-Paintrand, I.; Picart, C.; Auzély-Velty, R. Cyclodextrin/paclitaxel complex in biodegradable capsules for breast cancer treatment. *Chem. Mat.* **2013**, *25*, 3867−3873.
(23) Abd El-Rahman, M. K.; Mahmoud, A. M. A novel approach for spectrophotometric determination of succinylcholine in pharmaceutical formulation via host−guest complexation with water-soluble p-sulfonatocalixarene. *RSC Adv* **2015**, *5*, 62469−62476.
(24) Wang, Y.-X.; Guo, D.-S.; Duan, Y.-C.; Wang, Y.-J.; Liu, Y. Amphiphilic p-sulfonatocalix [4] arene as "drug chaperone" for escorting anticancer drugs. *Sci. Rep.* **2015**, *5*, 9019.
(25) Guo, D. S.; Liu, Y. Supramolecular chemistry of p-sulfonatocalix[n]arenes and its biological applications. *Acc. Chem. Res.* **2014**, *47*, 1925−1934.
(26) Roy, N.; Bomzan, P.; Ghosh, B.; Roy, M. N. A Combined Experimental and Theoretical Study on p-Sulfonatothiacalix [4] arene Encapsulated Sulisobenzone. *New J. Chem* **2023**, *47*, 1045−1049.
(27) Gao, S.; Bie, C.; Ji, Q.; Ling, H.; Li, C.; Fu, Y.; Zhao, L.; Ye, F. Preparation and characterization of cyanazine−hydroxypropyl-beta-cyclodextrin inclusion complex. *RSC Adv* **2019**, *9*, 26109−26115.
(28) Ghosh, B.; Roy, N.; Roy, D.; Mandal, S.; Ali, S.; Bomzan, P.; Roy, K.; Nath Roy, M. N. An extensive investigation on supramolecular assembly of a drug (MEP) with βCD for innovative applications. *J. Mol. Liq.* **2021**, *344*, 117977.
(29) Dallakyan, S.; Olson, A. J. Small-molecule library screening by docking with PyRx, Methods. *Mol. Biol.* **2015**, *1263*, 243−250.
(30) Abdel-Rahman, L. H.; Al−Farhan, B. S.; Al Zamil, N. O.; Noamaan, M. A.; El-Sayed Ahmed, H.; Adam, M. S. S. Synthesis, spectral characterization, DFT calculations, pharmacological studies, CT-DNA binding and molecular docking of potential N, O-multidentate chelating ligand and its VO(II), Zn(II) and ZrO(II) chelates. *Bioorg. Chem.* **2021**, *114*, 105106.
(31) Mandal, S.; Tarai, S. K.; Pan, A.; Bhaduri, R.; Biswas, P.; Moi, S. C. Cytotoxic effects of Pd(II) complexes on cancer and normal cells: Their DNA & BSA adduct formation and theoretical approaches. *Bioorg. Chem.* **2022**, *128*, 106093.
(32) Shedge, A. A.; Pansare, S. V.; Khairkar, S. R.; Chhatre, S. Y.; Chakrabarti, S.; Nagarkar, A. A.; Pansare, A. V.; Patil, V. R. Nanocomposite of functional silver metal containing curcumin biomolecule model systems: Protein BSA bioavailability. *J. Inorg. Biochem.* **2020**, *212*, 111210.
(33) Blois, M. S. J. N. Antioxidant determinations by the use of a stable free radical. *Nature* **1958**, *181*, 1199−1200.
(34) Haydar, M. S.; Das, D.; Ghosh, S.; Mandal, P. Implementation of mature tea leaves extract in bioinspired synthesis of iron oxide nanoparticles: preparation, process optimization, characterization, and assessment of therapeutic potential. *Chem. Pap.* **2022**, *76*, 491−514.
(35) Fu, W.; Chen, J.; Cai, Y.; Lei, Y.; Chen, L.; Pei, L.; Zhou, D.; Liang, X.; Ruan, J. Antioxidant, free radical scavenging, anti-inflammatory and hepatoprotective potential of the extract from Parathelypteris nipponica (Franch. et Sav.) Ching. *Ching. J. Ethnopharma.* **2010**, *130*, 521−528.
(36) Moein, M. R.; Moein, S.; Ahmadizadeh, S. J. M. Radical scavenging and reducing power of Salvia mirzayanii subfractions. *Mole* **2008**, *13*, 2804−2813.
(37) Gupta, S. K.; Islam, N.; Choudhuri, C.; Mandal, P. Elicitation of therapeutic potential and oxidative stress assessment of fenugreek sprouts under UV irradiation. *Int. J. Pharm. Pharm. Sci.* **2017**, *9*, 91−99.
(38) Shabbir, M.; Rashid Khan, M.; Saeed, N. Assessment of phytochemicals, antioxidant, anti-lipid peroxidation and anti-hemolytic activity of extract and various fractions of Maytenus royleanus leaves. *BMC Compl. Altern. Medi.* **2013**, *13*, 143.
(39) Ali, S.; Sikdar, S.; Basak, S.; Roy, D.; Dakua, V. K.; Adhikary, P.; Roy, M. N. High Visual Colorimetric Determination of F-Ions by Exploiting the Inhibition of Oxidase Mimicking Activity of FeMnO4@ GQD Nanocomposite. *Chem.Sel.* **2022**, *7*, No. e202201186.
(40) Wang, X.-X.; Wu, Q.; Shan, Z.; Huang, Q.-M. BSA-stabilized Au clusters as peroxidase mimetics for use in xanthine detection. *Biosen.sor. Bioelectro.* **2011**, *26*, 3614−3619.
(41) Mu, J.; Wang, Y.; Zhao, M.; Zhang, L. Intrinsic peroxidase-like activity and catalase-like activity of Co3O4 nanoparticles. *Chem. Comm.* **2012**, *48*, 2540−2542.
(42) Bomzan, P.; Roy, N.; Sharma, A.; Rai, V.; Ghosh, S.; Kumar, A.; Roy, M. N. Molecular encapsulation study of indole-3-methanol in cyclodextrins: Effect on antimicrobial activity and cytotoxicity. *J. Mol. Str.* **2021**, *1225*, 129093.
(43) Ol'khovich, M. V.; Sharapova, A. V.; Perlovich, G. L.; Skachilova, S. Y.; Zheltukhin, N. K. Inclusion complex of antiasthmatic compound with 2-hydroxypropyl-β-cyclodextrin: preparation and physicochemical properties. *J. Mol. Liq.* **2017**, *237*, 185−192.
(44) Roy, M. N.; Saha, S.; Barman, S.; Ekka, D. Host−guest inclusion complexes of RNA nucleosides inside aqueous cyclodextrins

https://doi.org/10.1021/acsomega.2c07396
ACS Omega 2023, 8, 6778−6790

explored by physicochemical and spectroscopic methods. *RSC Adv* **2016**, *6*, 8881−8891.
(45) Benesi, H. A.; Hildebrand, J. H. A spectrophotometric investigation of the interaction of iodine with aromatic hydrocarbons. *J. Am. Chem. Soc.* **1949**, *71*, 2703−2707.
(46) Zhang, W.; Gong, X.; Cai, Y.; Zhang, C.; Yu, X.; Fan, J.; Diao, G. Investigation of water-soluble inclusion complex of hypericin with β-cyclodextrin polymer. *Carbohydr. Polym.* **2013**, *95*, 366−370.
(47) Xiao, C. F.; Li, K.; Huang, R.; He, G. J.; Zhang, J. Q.; Zhu, L.; Yang, Q. Y.; Jiang, K. M.; Jin, Y.; Lin, J. Investigation of inclusion complex of epothilone A with cyclodextrins. *Carbohydr. Polym.* **2014**, *102*, 297−305.
(48) Yalkowsky, S. H.; Dannenfelser, R. M. *Aquasol database of aqueous solubility*; Version 5; University of Arizona TusconArizona-College of Pharmacy, 1992.
(49) Roy, N.; Ghosh, R.; Das, K.; Roy, D.; Ghosh, T.; Roy, M. N. Study to synthesize and characterize host-guest encapsulation of antidiabetic drug (TgC) and hydroxy propyl-β-cyclodextrin augmenting the antidiabetic applicability in biological system. *J. Mol. Str.* **2019**, *1179*, 642−650.
(50) Basu, M.; Sarkar, S.; Pande, S.; Jana, S.; Kumar Sinha, A. K.; Sarkar, S.; Pradhan, M.; Pal, A.; Pal, T. Hydroxylation of benzophenone with ammonium phosphomolybdate in the solid state via UV photoactivation. *Chem. Comm.* **2009**, *46*, 7191−7193.
(51) Patil, S. V.; Athare, S. V.; Jagtap, A.; Kodam, K. M.; Gejji, S. P.; Malkhede, D. D. Encapsulation of rhodamine-6G within p-sulfonatocalix[n]arenes: NMR, photophysical behaviour and biological activities. *RSC adv* **2016**, *6*, 110206−110220.
(52) Ashwin, B. C. M. A.; Vinothini, A.; Stalin, T.; Muthu Mareeswaran, P. Synthesis of a Safranin T -p-Sulfonatocalix[4]arene Complex by Means of Supramolecular Complexation. *Chem.Sel* **2017**, *2*, 931−936.
(53) Patil, S. V.; Gejji, S. P.; Kalyani, V. S.; Malkhede, D. D. Hydroxycoumarin encapsulated sulfonatothiacalix[4]arene: 1H NMR, steady state fluorescence and theory. *J. Mol. Liq.* **2021**, *339*, 116760.
(54) Saravanan, C.; Ashwin, B. C. M. A.; Senthilkumaran, M.; Mareeswaran, P. M. Supramolecular Complexation of Biologically Important Thioflavin-T with p-Sulfonatocalix[4]arene. *Chem. Sel* **2018**, *3*, 2528−2535.
(55) Rani, D.; Sethi, A.; Kaur, K.; Agarwal, J. Ultrasonication-Assisted Synthesis of a d-Glucosamine-Based β-CD Inclusion Complex and Its Application as an Aqueous Heterogeneous Organocatalytic System. *J. Org. Chem.* **2020**, *85*, 9548−9557.
(56) Valand, N. N.; Patel, M. B.; Menon, S. K. Curcumin-p-sulfonatocalix[4]resorcinarene (p-SC[4]R) interaction: thermo-physico chemistry, stability and biological evaluation. *RSC Adv* **2015**, *5*, 8739−8752.
(57) Ahmad, N.; Alam, M.; Al-Otaibi, M. A. N. Thermal decomposition and kinetic studies of solid riboflavin using model-free methods. *Prog. Reac. Kine. Mechan.* **2015**, *40*, 86−94.
(58) Narula, A.; Rao, C. P. Hydrogel of the Supramolecular Complex of Graphene Oxide and Sulfonatocalix[4]arene as Reusable Material for the Degradation of Organic Dyes: Demonstration of Adsorption and Degradation by Spectroscopy and Microscopy. *ACS Omega* **2019**, *4*, 5731−5740.
(59) Galindo-Murillo, R.; Sandoval-Salinas, M. E.; Barroso-Flores, J. In Silico Design of Monomolecular Drug Carriers for the Tyrosine Kinase Inhibitor Drug Imatinib Based on Calix- and Thiacalix[n]-arene Host Molecules: A DFT and Molecular Dynamics Study. *J. Chem. Theo. Comp.* **2014**, *10*, 825−834.
(60) Rehman, S. U.; Sarwar, T.; Husain, M. A.; Ishqi, H. M.; Tabish, M. Studying non-covalent drug-DNA interactions. *Arch. Biochem. Biophys.* **2015**, *576*, 49−60.
(61) Mandal, S.; Reddy B, V. P.; Mitra, I.; Mukherjee, S.; Tarai, S. K.; Bhaduri, R.; Pan, A.; Bose, K. J. C.; Ghosh, G. K.; Moi, S. C. Anticancer activity and biomolecular interaction of Pt (II) complexes: Their synthesis, characterisation and DFT study. *Appl. Organomet. Chem.* **2022**, *36*, No. e6506.
(62) Abdel-Rahman, L. H.; Abu-Dief, A. M.; El-Khatib, R. M.; Abdel-Fatah, S. M. Some new nano-sized Fe(II), Cd(II) and Zn(II) Schiff base complexes as precursor for metal oxides: Sonochemical synthesis, characterization, DNA interaction, in vitro antimicrobial and anticancer activities. *Bioorg. Chem.* **2016**, *69*, 140−152.
(63) Abeydeera, N.; Perera, I. C.; Perera, T. Synthesis, Characterization, and BSA-Binding Studies of Novel Sulfonated Zinc-Triazine Complexes. *Bioinorg. Chem. Appl.* **2018**, *2018*, 7563820.
(64) Anjomshoa, M.; Fatemi, S. J.; Torkzadeh-Mahani, M.; Hadadzadeh, H. DNA- and BSA-binding studies and anticancer activity against human breast cancer cells (MCF-7) of the zinc(II) complex coordinated by 5,6-diphenyl-3-(2-pyridyl)-1,2,4-triazine, Spectrochim. Acta Part A. *Mol. Biomol. Spectrosc.* **2014**, *127*, 511−520.
(65) Ashoori, M.; Saedisomeolia, A. Riboflavin (vitamin B2) and oxidative stress: a review. *Brit. J. Nutri.* **2014**, *111*, 1985−1991.
(66) Sudirman, S.; Nurjanah, N.; Jacoeb, A. Proximate compositions, bioactive compounds and antioxidant activity from large-leafed mangrove (Bruguiera gymnorrhiza) fruit. *Int. Food Res. J.* **2014**, *21*, 2387.
(67) Minotti, G.; Aust, S. D. The requirement for iron (III) in the initiation of lipid peroxidation by iron (II) and hydrogen peroxide. *J. Bio. Chem.* **1987**, *262*, 1098−1104.
(68) Venuti, V.; Crupi, V.; Fazio, B.; Majolino, D.; Acri, G.; Testagrossa, B.; Stancanelli, R.; De Gaetano, F.; Gagliardi, A.; Paolino, D. J. B.; Floresta, G.; Pistarà, V.; Rescifina, A.; Ventura, C. A. Physicochemical characterization and antioxidant activity evaluation of idebenone/hydroxypropyl-β-cyclodextrin inclusion complex. *Biomolecules* **2019**, *9*, 531.
(69) Ali, S.; Sikdar, S.; Basak, S.; Das, D.; Roy, D.; Salman Haydar, M. S.; Kumar Dakua, V. K.; Adhikary, P.; Mandal, P.; Nath Roy, M. N. Synthesis of β-cyclodextrin grafted rhombohedral-CuO antioxidant nanozyme for detection of dopamine and hexavalent chromium through off−on strategy of peroxidase mimicking activity. *Microchem. J.* **2022**, *179*, 107514.
(70) Gao, L.; Zhuang, J.; Nie, L.; Zhang, J.; Zhang, Y.; Gu, N.; Wang, T.; Feng, J.; Yang, D.; Perrett, S.; Yan, X. Intrinsic peroxidase-like activity of ferromagnetic nanoparticles. *Nat. nanotech.* **2007**, *2*, 577−583.

https://doi.org/10.1021/acsomega.2c07396
ACS Omega 2023, 8, 6778−6790